Check for updates

Femtosecond Laser Nanomachining of High-Aspect-Ratio Channels in Bulk Fused Silica

*Pasquale Barbato, Roberto Osellame, and Rebeca Martínez Vázquez**

Thee-dimensional nano-structuring of bulk fused silica glass remains a challenging issue due to limitations of traditional fabrication methods. In the present work the fabrication of hollow mm-length channels is demonstrated in bulk fused silica by femtosecond laser irradiation followed by chemical etching, achieving feature sizes of 300 nm. The tight focusing and threshold energy conditions allow to reveal unexplored fabrication regimes. The robustness and repeatability of the process are demonstrated through the fabrication of fused silica diffraction gratings, made of parallel hollow channels with variable pitches even in the sub-wavelength regime.

1. Introduction

Ultrafast laser-processed fused silica[1,2] has proved to be a top-choice platform for integrated photonic circuits and lab-on-a-chip applications, due to its unique properties. In fact, fused silica glass has a large transparency range in the electromagnetic spectrum ranging from ultraviolet (≈200 nm) to infrared (≈2500 nm),[3] presents weak self-fluorescence, is mechanically and chemically stable and highly resistant to thermal stresses. In recent years many efforts have been made to gain both understanding and control of chemical-assisted manufacturing of hollow 3D structures in bulk fused silica.[4–7] The intrinsically 3D nature of the technique has empowered the development of integrated networks of hollow channels with applications in a variety of fields like optofluidics, lab-on-chip,[8–10] sensing[11] or more recently in extreme laser physics[12,13] and fiber optics.[14,15] The technique, usually referred to as Femtosecond Laser Irradiation followed by Chemical Etching (FLICE), is a two-step process. First, a train of femtosecond pulses, with a central wavelength in the visible or the near-infrared, is focused inside a fused silica sample. Here, the photons can be non-linearly absorbed by the material, mainly through multiphoton absorption and avalanche ionization.[16,17] The resulting photo-excited electron plasma relaxes, leaving a local permanent modification of the material, which is governed by the focusing and irradiation parameters.[18]

The final modification can be roughly classified into three rather different groups: a positive change in refractive index change of the material (type I), an enhancement of the etching rate of the irradiated volume due to the formation of the so-called "nanogratings" (type II), and the formation of voids (type III).[18,19] Traditionally, type II modifications are one of interest for FLICE: By moving the sample with respect to the laser focus, it is possible to create 3D patterns inside bulk fused silica which are subsequently etched by a proper chemical agent thus creating embedded empty channels. These inscriptions can go from straight lines, which results in buried hollow channels and tunnels[4] to more complicated and carefully engineered 3D designs, allowing the realization of truly integrated lab-on-a-chip devices.[15,16]

Chemical etching selectivity promoted by femtosecond laser irradiation is strongly dependent on the type of chosen chemical agent. Hydrofluoric acid (HF) solutions are widely used in research activities, showing etching contrasts up to 1:100 and etching rates of ≈300 μm h^{-1} of the irradiated tracks.[4] The cause for this high chemical selectivity in HF is believed to be the formation, during irradiation, of subwavelength nanoplanes of highly densified material, arranged in a nanograting configuration and oriented orthogonally to laser polarization. The alignment of these nanogratings along the irradiated track promotes the etching into a hollow channel.[20–22] Alkaline aqueous solutions, like potassium hydroxide (KOH) and sodium hydroxide (NaOH) constitute a less hazardous alternative to HF for FLICE. As Casamenti et al.[23] recently demonstrated for both etchants, it is possible to achieve etching rates comparable to HF solutions (≈300 μm h^{-1}) but they present a significantly higher etching contrast, ≈1:300 for KOH and even 1:600 for NaOH. These high etching contrasts improve FLICE resolution, enabling channel cross-sections of a few micrometers along several millimeters of channel length.[23,24]

In the case of alkaline solutions in addition to nanograting formation, structural modifications such as the presence of defects like non-bridging oxygen holes (NBOHC) and oxygen deficiency centers (ODC) are the primary reasons driving the

P. Barbato, R. Osellame, R. Martínez Vázquez
Institute for Photonics and Nanotechnologies
National Research Council (IFN-CNR)
Piazza Leonardo da Vinci 32, Milan 20133, Italy
E-mail: rebeca.martinezvazquez@cnr.it

P. Barbato
Physics Department
Politecnico di Milano
Piazza Leonardo da Vinci 32, Milan 20133, Italy

The ORCID identification number(s) for the author(s) of this article can be found under https://doi.org/10.1002/admt.202400240

© 2024 The Authors. Advanced Materials Technologies published by Wiley-VCH GmbH. This is an open access article under the terms of the Creative Commons Attribution License, which permits use, distribution and reproduction in any medium, provided the original work is properly cited.

DOI: 10.1002/admt.202400240

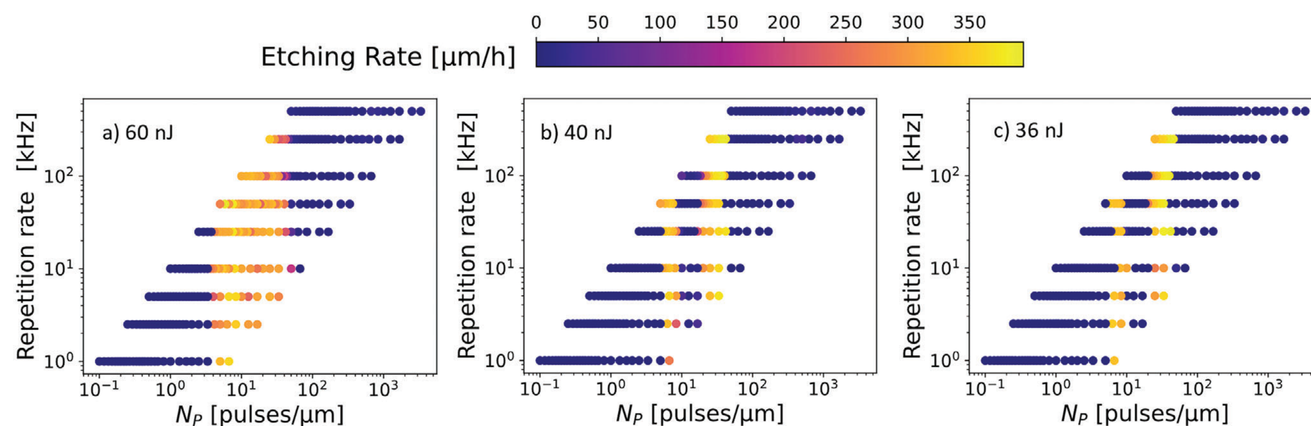

Figure 1. The etching rate of the irradiated tracks at a pulse energy of 60 nJ a), 40 nJ b) an 36 nJ c). Values for different repetition rates are reported as a function of the number of pulses per micrometer, revealing two different etching regions.

etching increase.[23] Moreover, recent findings by Ochoa et al.[22] have demonstrated the independence of etching in NaOH from laser polarization in the few pulses regime, thus strengthening this theory.

The nano-structuring of hollow voids or channels in fused silica by FLICE would be very attractive to support 3D nanofluidic research[26,27] or in nano-photonics applications.[28] Still, the realization of nanochannels in fused silica, despite some preliminary interesting results,[29,30] is challenging mainly due to the characteristics of the process. The cross-section of the channels fabricated by FLICE is influenced by the laser-focusing conditions and the etching selectivity. The dimensions of the modified voxel are mainly governed by the focusing conditions and related spherical aberrations due to refractive index mismatch between the external media and the material. Afterward, the profile of this voxel further increases due to the etching of the pristine material. Consequently, for what concerns fused silica, the typical hollow structures fabricated by FLICE present profiles ranging from tenths to hundreds of micrometers, in channels with lengths of some millimeters and even centimeters.

In this work, we propose a new femtosecond laser irradiation regime to locally modify fused silica chemical etching at the nanoscale. Exploiting high-focusing conditions, irradiation at energy threshold, and highly selective etching conditions we realize sub-micrometric hollow channels in bulk fused silica. The stability of this new regime is demonstrated by the fabrication of high-density diffractive gratings with sub-micrometer pitches.

2. Results

To investigate the likelihood of obtaining empty channels with submicrometer cross sections in fused silica, by the FLICE technique, we make a preliminary selection of the irradiation conditions promoting the smallest modified volume. The 515 nm wavelength laser beam is focused inside the fused silica slabs by a high numerical aperture glycerine immersion microscope objective (NA = 1.35). This immersion ensures an almost perfect refractive index matching with fused silica (≈1.46), thus minimizing spherical aberrations which will induce an elongation in the depth of the laser-modified voxel.[31] Under these conditions, we can estimate to have an almost spherical focal spot with a submicrometer waist. The focus is located 150 µm under the substrate surface which is moved perpendicularly to the laser beam. We explore laser repetition rates (RRs) lower than or equal to 500 kHz to prevent thermal accumulation effects[32] and energies near the laser modification threshold (experimentally found to be 30 nJ ± 2 nJ for the above irradiation conditions). After irradiation, the samples were immersed in a NaOH aqueous solution, which is known to give the highest selectivity for fused silica etching.

Our rationale is to study the material etching using the lowest exposure conditions, thus varying the translation speed for each combination of repetition rate and near-threshold pulse energies. We explored 28 velocities between 0.15 mm s^{-1} and the maximum speed allowed by the movement system (10 mm s^{-1}). A satisfactory value to parametrize the laser exposure in this study is the number of delivered pulses for unit length (N_P), calculated as the ratio between laser RR and sample translation speed.

Figure 1 reports the etching rates for three pulse energies, for all the laser repetition rates and N_P under study. For a pulse energy of 60 nJ etching is observed for N_P approximately between 6 and 40 pulses µm^{-1}, while etching does not start for values outside this interval (Figure 1a), regardless of the laser RR. In this interval, the average value of the etching rate is 200 ± 78 µm h^{-1}, but it reaches values up to 383 µm h^{-1} at both sides of the range, while it can be as low as 124 µm h^{-1} in the central part. This behavior is more evident for lower pulse energies (Figure 1b,c 40 and 36 nJ). Here, in the central part, the etching rate is almost negligible, and it is surrounded by two tight regions with etching rates exceeding 350 µm h^{-1}, with this latter value comparable to the highest fused silica etching rates found in the literature for NaOH.[21]

The top-view optical microscope images of the irradiated tracks at 36 nJ, after etching, in the relevant interval of N_P are presented in **Figure 2a**. In this case, the repetition rate is kept fixed at 10 kHz while the sample translation speed decreases, thus increasing N_P. A magnification of the non-etched tracks (Figure 2b) reveals that those lines are made of periodically distributed modified regions, surrounded by apparently non-modified material. The distance between these spots decreases with N_P, thus decreasing

 © 2024 The Authors. Advanced Materials Technologies published by Wiley-VCH GmbH

2365709x, 2024, 18, Downloaded from https://onlinelibrary.wiley.com/doi/10.1002/admt.202400240 by POLITECNICO DI MILANO, Wiley Online Library on [18/09/2024]. See the Terms and Conditions (https://onlinelibrary.wiley.com/terms-and-conditions) on Wiley Online Library for rules of use; OA articles are governed by the applicable Creative Commons License

2365709x, 2024, 18, Downloaded from https://onlinelibrary.wiley.com/doi/10.1002/admt.202400240 by POLITECNICO DI MILANO, Wiley Online Library on [18/09/2024]. See the Terms and Conditions (https://onlinelibrary.wiley.com/terms-and-conditions) on Wiley Online Library for rules of use; OA articles are governed by the applicable Creative Commons License

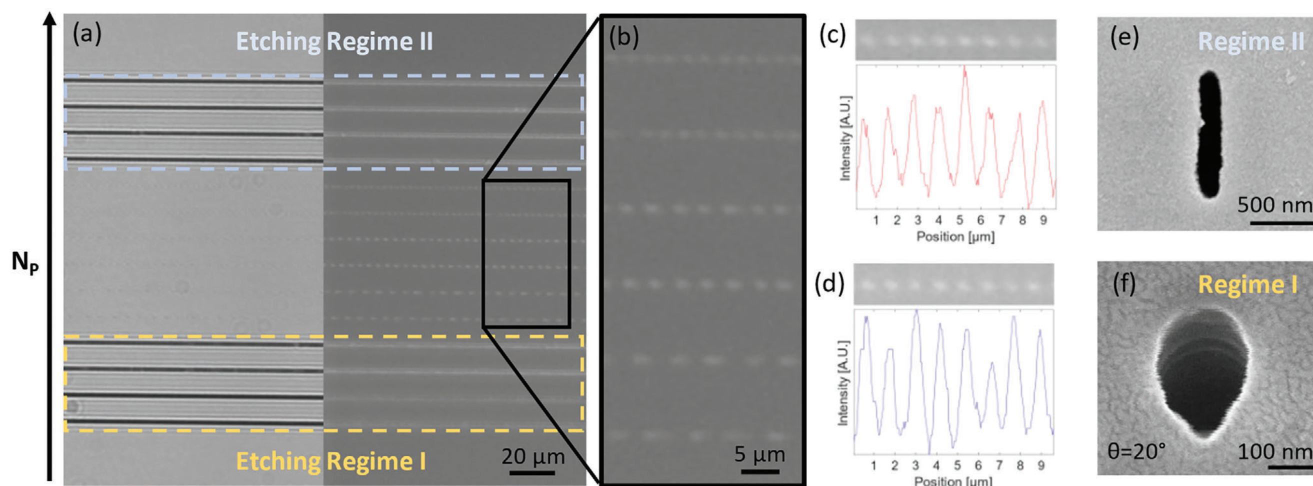

Figure 2. a) Optical microscope top-view image of the sample after irradiation and etching. The irradiation is performed at 36 nJ, at a fixed repetition rate (10 kHz), and for decreasing writing velocities (from 1.25 to 0.30 mm s^{-1} from bottom to top), corresponding to an increase of the number of pulses per µm (N_P). Two lines are irradiated for each velocity. The two etching regimes are visible as high-contrast black lines separated by a non-etching region. The image is obtained with 40X magnification objective both in a transmission (left) and reflection (right) incidence of the illuminating light. Although this image refers to a specific RR, it is representative of all the data in Figure 1c; b) An enlargement of the etching gap which makes visible the periodic nature of this modification; Modification profiles of the periodic pattern for c) RR = 25 kHz and 1.5 mm s^{-1} and d) RR = 50 kHz and 3 mm s^{-1}, showing that the periodicity is independent of the repetition rate. Cross-section Scanning Electron Microscopy images of the entrance of a representative nanochannel: e) for regime II (36 nJ, 25 kHz, 3 mm s^{-1}) and f) regime I (30 nJ, 25 kHz, 3 mm s^{-1}). This latter is the smallest channel entrance we produced, with a horizontal dimension of ≈220 nm and a vertical one ≈340 nm The image is captured with the sample tilted at 20°, to partially show the inside of the channel.

the translation velocity. The intensity profile along the irradiated track of two microscope images at different repetition rates are reported in Figure 2c,d, they show that regardless of laser repetition rate (25 and 50 kHz, respectively) and translation speed (1.5 and 3 mm s^{-1}, respectively), the periodicity is the same for equal number of laser pulses per spot (≈16 pulses µm^{-1}). It is worth noting that the spacing of the dots in these lines is not equal to the spacing of subsequent laser pulses, which are well overlapped also in this regime. Additionally, we observe that a less selective etchant (i.e., HF) would not reveal this etching gap because of a more efficient etching of unmodified material in these tracks.

Scanning Electron Microscopy (SEM) images of the cross-section of etched channels from the regimes surrounding the gap (Figure 2e,f), reveals that they are effectively empty and that they have submicrometer dimensions with quite different profiles. In regime I (for low N_p) there is an almost circular profile with a diameter ≈300 nm, while in regime II (higher N_p) we see an elongated modification with 162 nm width and 955 nm height.

From Figure 2f, it is possible to appreciate a partial view of the interior of the channel, which appears empty. To further reinforce the assertion that these channels are indeed hollow throughout their entire length, we cut a sample to expose their inner walls. The procedure and results of this experiment are detailed in the supplementary text. Figure S1 (Supporting Information) shows the interior surfaces at various positions along the channel, confirming not only their emptiness but also that they maintain a constant profile and a roughness on the order of a few tens of nanometers. The different cross-section profiles of Figure 2e,f reveals an intrinsically different nature of the modification behind the two regimes. As a further test, we repeat the experiment at 50 kHz and the same set of translation speeds, but with the polarization parallel to the writing direction. Remarkably, Regime II seems the only one to be affected by laser polarization direction, while in Regime I we can obtain etching rates comparable to the ones obtained with a perpendicular polarization.

In both etching regimes, the final length of the channel can be as high as 1 mm, giving rise to nanochannels with aspect ratios of the order of 10^4.

Once demonstrated the fabrication of sub-micrometer feature-size hollow structures, we aim to verify the reproducibility and robustness of this process to ensure its viability for real-world applications. Thus, as a proof of concept, we fabricated optical volume diffraction gratings with different pitches. In a glass sample with a footprint of 20 mm in length and 2 mm in width, four distinct diffraction gratings were realized inscribing a total of 48 000 lines with the irradiation parameters of the previously defined regime I. The whole inscription process lasted ≈9 h and no significant variations in the final modification were observed during this amount of time. The sample is subsequently immersed in a NaOH aqueous solution for 3 h, allowing the chemical agent to etch from both sides of the sample, leading to the formation of pass-through nanochannels.

SEM pictures of the side cross-sections of the nanochannels are shown in **Figure 3**. Two of them present a pitch of 500 nm (Figure 3a) while the latter two have a pitch of 1000 nm (Figure 3b). The difference between the two gratings with the same pitch is the height of the nanochannels: one is made by a single laser scan, while the second is created with three scans separated by 300 nm in depth, proving the robustness of the process and the ability to create gratings of arbitrary thickness. To provide a more quantitative assessment of the reproducibility of the resulting channels, we measured the vertical and horizontal

 © 2024 The Authors. Advanced Materials Technologies published by Wiley-VCH GmbH

2365709x, 2024, 18, Downloaded from https://onlinelibrary.wiley.com/doi/10.1002/admt.202400240 by POLITECNICO DI MILANO, Wiley Online Library on [18/09/2024]. See the Terms and Conditions (https://onlinelibrary.wiley.com/terms-and-conditions) on Wiley Online Library for rules of use; OA articles are governed by the applicable Creative Commons License

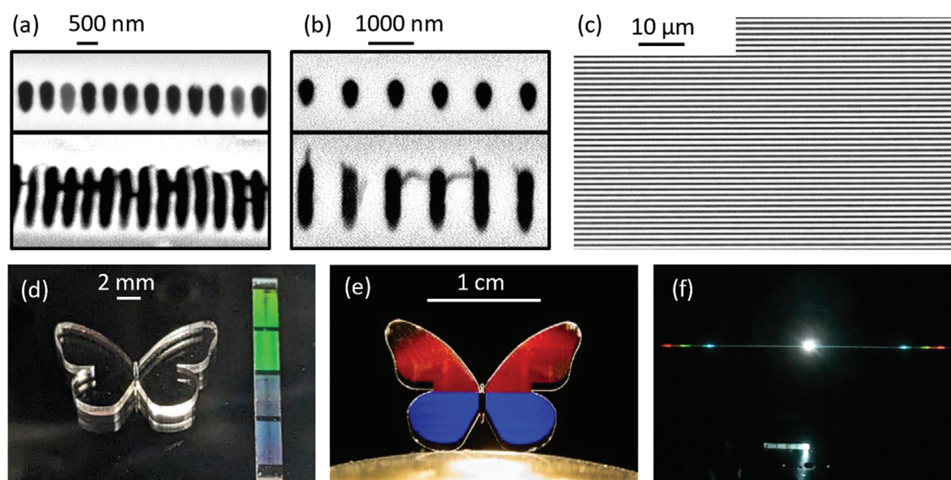

Figure 3. a,b) Scanning Electron Microscope images of the lateral facet of diffraction gratings realized with a pitch of 500 and 1000 nm, respectively. c) Top-view at the optical microscope of 1000 nm-pitch diffraction grating. d) Picture of hollow nanochannels acting as diffraction gratings in a fused silica slab (right) reflecting ambient light and a butterfly-shaped sample (left) in which femtosecond laser tracks are only irradiated but not etched. e) Diffraction of white light from the irradiated tracks in the butterfly-shaped sample f) Diffraction of a polycromatic beam propagating through the nanomachined fused silica slab sample.

dimensions of the profiles depicted in the upper panel of Figure 3b. The measurements yielded values of 607 ± 21 nm for the vertical dimension and 360 ± 8 nm for the horizontal dimension, respectively.

It should be observed that multiple laser scan gratings suffer from the increased energy absorbed by the material, which induces stress in the material, resulting in randomly distributed cracks after etching. This is particularly evident in the case of a 500 nm pitch grating with triple scanning, where the glass thickness separating individual channels, ≈200 nm, is frequently traversed by nanometric-size fractures.

A top view of the 1000 nm-pitch single-scan grating taken at an optical microscope with a 40x objective is shown in Figure 3c. The high contrast between the etched tracks and the unmodified material suggests that we are uniformly producing hollow nanochannels.

We can infer the effective emptiness of the nanochannels by comparing their diffraction efficiency before and after etching. To do so, the etched gratings are placed next to a butterfly-shaped sample (Figure 3d), in the wings of which traces with a pitch of 800 and 600 nm are inscribed but have not been etched. When placed under white ambient light, the 1000 and 500 nm gratings show a diffractive behavior, brightly reflecting the different components at different angles. This diffraction is not always uniform along their length (see top grating in Figure 3d), suggesting that not all channels have been completely etched in the central region, especially in the case of gratings produced with triple scanning. In contrast, the butterfly-shaped sample remains transparent under the same illuminating conditions. However, the presence of the traces in the wings can be revealed by placing a focused intense white light source under the sample, obtaining the picture in Figure 3e. This behavior can be explained by considering that laser absorption induces a small change in the refractive index, which becomes much more significant when the channels are emptied, given the higher index contrast between air and fused silica (n = 1.46). This higher refraction index contrast reflects a higher diffraction efficiency, as predicted by the coupled wave theory for volume diffraction gratings.[33,34]

The proper functioning of the volume gratings is demonstrated by directing a laser beam and looking at the transmitted diffracted orders. When a polychromatic laser beam impinges on the 1000 nm-pitch grating we obtain a spatial separation of the different spectral components, with higher frequencies diffracted at larger angles, as predicted by Bragg's law (Figure 3f). A wavelength of 600 nm is then selected and directed onto the four gratings, and the diffraction efficiency in the first order is measured. For the 500 nm-pitch gratings, all the power is transmitted into zero order and no diffraction is revealed since they act as a sub-wavelength diffraction grating, while the 1000 nm-pitch single-scan and triple-scan diffract 15,0% and 21,6% of the impinging power into ±1 orders. These efficiencies are in good agreement with the values obtained from computational simulations with Comsol (see Supplementary Material) and further demonstrate the emptiness of the single channel.

3. Discussion

In the present work, we demonstrate that long, submicrometric profile hollow channels can be fabricated in bulk fused silica by NaOH wet chemical etching promoted by irradiation with tightly focused femtosecond laser beams. To the best of our knowledge, this is the first time that empty channels with mm length and nanometer-sized cross sections have been fabricated in fused silica by the FLICE technique.

We found etching rates in good agreement with the ones in literature[24,25] and confirmed the polarization-insensitive etching region found by Ochoa et al.[25] Interestingly there are two unexpected drops in the etching rates, the first one features the transition between the polarization-dependent and non-dependent etching (N_P ≈6–9 pulses μm^{-1}), while the last one (at N_P ≈36 pulses μm^{-1}) happens to be the etching limit which appears at fairly low pulse densities. We believe that this

© 2024 The Authors. Advanced Materials Technologies published by Wiley-VCH GmbH

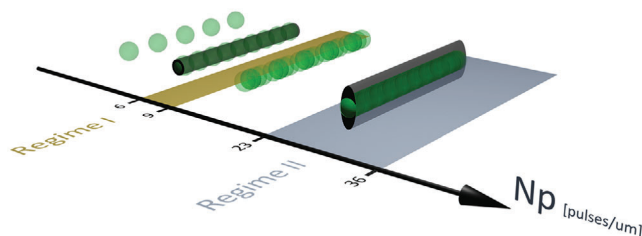

Figure 4. Schematic illustration of the laser modification for an increasing number of pulses per unit length (N_p). The weak green spheres represent the modified voxel, while the continuous gray regions represent the material where etching is present. From left to right: for $N_p < 6$ pulses μm^{-1}, nonlinear absorption occurs in spatially separated spots. Between ≈6 and 9 pulses μm^{-1}, the concatenation of individual modifications aligns to form a single track, effectively etched into a nanochannel identified as regime I. As the number of pulses increases, the cumulative absorption of multiple pulses in the same spot gives rise to a different type of modification, initially not continuous but spatially localized. For more than ≈23 pulses μm^{-1}, the modification becomes continuous, resulting in what is usually called a "nanograting" that can be selectively etched. For $N_p > 36$ the excessive number of pulses per unit length spoils the nanograting formation and consequently prevents etching.[38]

interesting behavior is a consequence of the irradiation conditions used in the present work. If we compare our laser spot dimensions with other works dealing with NaOH etching promoted by laser irradiation[24,25] we are using a beam waist at the focus almost four times smaller (≈500 nm compared to ≈1.9 µm) thus for the same pulse energy and translation speed conditions we will have four times higher fluence. This, combined with the low spherical aberrations during beam focusing, gives a favorable situation for locally induced fused silica ordered and disordered nanogratings even for a few pulses' absorption.

Although an in-depth analysis of laser-material interaction is left to future work, based on the experiments here described we can give a qualitative interpretation of our findings, which we graphically summarized in **Figure 4**.

1) At very high translation speeds N_p is too low, and it does not allow to have voxel superposition along the translation direction consequently, we will obtain a non-continuous modification that prevents the etching of the tracks. We experimentally found that this happens for $N_p < 6$ pulses μm^{-1}, which implies a voxel dimension before the etching of ≈150 nm.
2) For pulse densities slightly higher than 6 pulses μm^{-1}, the modification becomes continuous along the scanning direction with an increasing, but small, superposition between the subsequent voxels. Here, we reach an etching rate of ≈300 $\mu m\, h^{-1}$. The fact that we are in a regime with a very small overlap between voxels and the observation of the etching rate independent from the laser polarization suggests that the etching is due to the presence of point defects in fused silica like E' centers, non-bridging oxygen hole centers (NBOHC), and divalent silicon with oxygen deficiency centers,[35,36] and not to the creation of nanogratings that need a strong overlap of subsequent pulses to be formed.
3) At a certain point, the increasing superposition between voxels will induce the incubation of these defects through a cumulative pulse absorption event. This will lead to nanoplanes formation, with a process analogous to the transient nanoplasmonic model proposed by Taylor et al. [37] Here, this regime starts for a low pulse density ($N_p \approx 9$ pulses μm^{-1}) due to the high energy density achieved in our extreme focusing condition. For pulse energies near the threshold, we have an etching drop up to $N_p \approx 20$ pulses μm^{-1}. Below this value, the number of pulses per unit length is not sufficient to sustain the uniform creation of nanogratings that require a given incubation length before forming; once the nanograting is formed the incubation is interrupted and it needs to restart. This results in a periodical pattern of regions with nanogratings and almost unmodified material. Dividing N_p by the distance between two spots we can estimate that at least 3 partially overlapped pulses are needed to induce the incubation effect that will give nanograting formation. For higher energies, the number of pulses needed to induce this nanograting creation is lower and we do not see this drop in etching rate.
4) For more than 20 pulses μm^{-1}, the process of nanograting formation becomes stable giving rise to a continuous track. The etching process becomes effective again (we previously called this condition the etching Regime II). In this regime the nanochannel cross sections show an elongation in the beam propagation direction induced by the pulse cumulative nature of the modification.
5) When increasing even more the pulse density we reach an absorption regime where the number of delivered pulses in the same voxel becomes excessively high and the modification track presents no etching due to a disordering of the nanogratings.[38]

With these results, we are setting the base for a fast and precise nano-machining in the volume of fused silica by the FLICE technique. Here we demonstrate long empty nanochannels used as optical diffraction gratings, but we envisage the possibility of creating more complicated 3D nanochannel networks to obtain, e.g., hollow-core photonic crystal waveguides[28] or even Extreme Ultraviolet metaoptics.[39]

4. Experimental Section

The laser beam was provided by an air-cooled femtosecond Yb-doped fiber laser (Satsuma, Amplitude Systems S.A.), delivering 260 fs-long pulses at a central wavelength of 1030 nm and with a variable repetition rate from single shot to 40 MHz. At 1 MHz, it provides a maximum power of 10 W, tunable with an internal attenuator. Its long-term mean power stability was <1% rms over 100 h, which was adequate to ensure good reproducibility of the results. In fact, under the irradiation conditions used for the inscription of the gratings, it was measured that a mean power variation of ≈6% results in a variation in channel cross-section dimensions of less than 50 nm.

To guarantee optimum operating conditions, the temperature of the room was held at 22 ± 1 °C and humidity ≈40%.

The wavelength of the beam was halved through second harmonic generation in a LBO crystal and was then directed to the inscription stages, where it was focused on the fused silica substrate (Corning 7980 Standard Grade) through a glycerine-immersion 150x objective (Zeiss, Plan-Apochromat) with a numerical aperture (NA) of 1.35. The dimension of the laser beam was increased with a beam expander to slightly overfill the objective entrance and take full advantage of the high numerical aperture. The high NA results in a short working distance, which, according to specifications provided by the manufacturer, was 330 µm. All the data reported in this work refer to an inscription depth of 150 µm, but we had also

© 2024 The Authors. Advanced Materials Technologies published by Wiley-VCH GmbH

2365709x, 2024, 18, Downloaded from https://onlinelibrary.wiley.com/doi/10.1002/admt.202400240 by POLITECNICO DI MILANO, Wiley Online Library on [18/09/2024]. See the Terms and Conditions (https://onlinelibrary.wiley.com/terms-and-conditions) on Wiley Online Library for rules of use; OA articles are governed by the applicable Creative Commons License

experimentally confirmed that it was possible to modify the material until a depth of 300 µm from the upper surface of the sample. The glycerine immersion was chosen to minimize spherical aberrations, as its refractive index (n = 1.456 at 23 °C) was close to the substrate's (n = 1.460). The objective was mounted on a pneumatic 1D translational stage (Aerotech, ANT130-035-L-ZS-PLUS), allowing the translation of the focus on the z-axis, while the sample lies on a two-axis stage (Aerotech, ANT95-50-XY-CMS-ULTRA) for the movement in the XY plane. These high-precision stages ensure a control of the relative positioning between the sample and the focal volume with a resolution of less than 10 nm. The maximum possible translation speed was 10 mm s^{-1}. The beam power was measured right before the objective lens. To determine the laser modification threshold, irradiations were performed at decreasing powers until the modifications were no longer visible at the optical microscope.

The irradiation of the straight lines for the etching rate measurement was done by translating the sample always in the same direction in order to avoid quill effects.[40] The laser beam polarization was always linear and perpendicular to the irradiation direction, unless for the polarization etching test, where the polarization was rotated by a half-waveplate along the scanning direction. In each experiment, two 3 mm long lines were inscribed with the same irradiation parameters at a distance of 5 µm. The etching rates shown in this paper were always the average of four different measurements, and, in particular, the data in Figures 1a–c have an average standard deviation of 48, 8, and 4 µm h^{-1}, respectively.

The outer frame of the 2 mm slab -samples, see Figure 3 panels from (a) to (d) and (f) are realized with the FLICE technique, prior to the inscription of the volume diffraction gratings. The setup was the same as described above, but a RR of 1 MHz and a power of 300 mW were used. The laser was focused with a 63X Zeiss dry objective (LD-plan Neofluor), NA = 0.65, and the etching was performed with a 20% HF aqueous solution. After creating the outer shape, straight lines were inscribed into the sample using the methodology explained earlier with variable pitches.

After the irradiations, the two lateral facets of the samples were polished to remove the effects of non-uniformly irradiated regions and acceleration/deceleration of the movement stages close to the sample edges. The samples were subsequently immersed for 3 h in a 1 M NaOH aqueous solution at 65 ± 5 °C with an analogic magnetic stirrer.

The butterfly-shaped sample of Figure 3d,e was realized first by inscribing the outer profile and subsequent etching with HF. Afterward, diffraction gratings were inscribed inside this butterfly frame that, however, did not undergo NaOH etching.

Finally, the samples were analyzed under an optical microscope (Nikon Eclipse me600) in transmission and reflection mode, to study the morphology of the irradiated lines and to measure the etching rates. The profile of the etched tracks was then analyzed using scanning electron microscopy (Thermo Scientific Phenom Pro and LEO 1525 / Raith Elphy Plus). This last measurement was performed after the deposition of a 5 nm layer of gold over the glass surface with a sputter coater (Cressington Sputter Coater 108auto).

A tunable visible fiber laser (FemtoFiber pro TVIS, Toptica), with a wavelength ranging from 480 to 640 nm, was utilized to characterize the diffractive behavior of the volume Bragg gratings.

Supporting Information

Supporting Information is available from the Wiley Online Library or from the author.

Acknowledgements

The authors would like to thank Dr. Pablo Roldan for fruitful discussion regarding NaOH etching, and Dr. Elisa Sogne for the assistance in the acquisition of SEM images at the PoliFab facility. This research has received funding from the European Union Horizon 2020 Research and Innovation Program under Grant Agreement No. 964588 (XPIC),

Conflict of Interest

The authors declare no conflict of interest.

Data Availability Statement

The data that support the findings of this study are openly available in [ZENODO] at [https://zenodo.org/], reference number [11060617].

Keywords

femtosecond laser micromachining, fused silica glass, nanochannels, subwavelength diffractive gratings

Received: February 13, 2024
Revised: April 10, 2024
Published online: May 16, 2024

[1] K. M. Davis, K. Miura, N. Sugimoto, K. Hirao, *Opt. Lett.* **1996**, *21*, 1729.
[2] A. Marcinkevicius, S. Juodkazis, M. Watanabe, M. Miwa, S. Matsuo, H. Misawa, J. Nishii, *Opt. Lett.* **2001**, *26*, 277.
[3] Datasheet: Corning ® HPFS ® 7979, 7980, 8655 Fused Silica Optical Materials Product Information, https://www.corning.com/media/worldwide/csm/documents/HPFS_Product_Brochure_All_Grades_2015_07_21.pdf on 09/04/2024.
[4] Y. Bellouard, A. Said, M. Dugan, P. Bado, *Opt. Express* **2004**, *12*, 2120.
[5] Y. Shimotsuma, K. Hirao, P. G. Kazansky, J. Qiu, *Jpn. J. Appl. Phys.* **2005**, *44*, 4735.
[6] R. R. Gattass, E. Mazur, *Nat. Photonics* **2008**, *2*, 219.
[7] K. C. Vishnubhatla, N. Bellini, R. Ramponi, G. Cerullo, R. Osellame, *Opt. Express* **2009**, *17*, 8685.
[8] K. Sugioka, Y. Cheng, *Lab Chip* **2012**, *12*, 3576.
[9] R. Osellame, H. J. W. M. Hoekstra, G. Cerullo, M. Pollnau, *Laser Photon Rev* **2011**, *5*, 442.
[10] F. Sima, K. Sugioka, R. Martínez Vázquez, R. Osellame, L. Kelemen, P. Ormos, *Nanophotonics* **2018**, *7*, 613.
[11] H. E. Parker, S. Sengupta, A. V. Harish, R. R. G. Soares, H. N. Joensson, W. Margulis, A. Russom, F. Laurell, *Sci. Rep.* **2022**, *12*, 3539.
[12] A. G. Ciriolo, R. Martínez Vázquez, G. Crippa, M. Devetta, D. Faccialà, P. Barbato, F. Frassetto, M. Negro, F. Bariselli, L. Poletto, V. Tosa, A. Frezzotti, C. Vozzi, R. Osellame, S. Stagira, *Photonics* **2022**, *7*, 110801.
[13] M. Galli, V. Wanie, D. P. Lopes, E. P. Månsson, A. Trabattoni, L. Colaizzi, K. Saraswathula, A. Cartella, F. Frassetto, L. Poletto, F. Légaré, S. Stagira, M. Nisoli, R. Martínez Vázquez, R. Osellame, F. Calegari, *Opt. Lett.* **2019**, *44*, 1308.
[14] K. Ehrlich, C. A. Ross, R. J. Beck, J. D. Shephard, R. R. Thomson, *APL Photonics* **2023**, *8*, 076109.
[15] C. A. Ross, K. Harrington, R. Mears, J. M. Stone, T. M. Birks, R. R. Thomson, *Opt. Express* **2024**, *32*, 922.
[16] C. B. Schaffer, A. Brodeur, E. Mazur, *Meas. Sci. Technol.* **2001**, *12*, 1784.
[17] D. M. Rayner, A. Naumov, P. B. Corkum, *Opt. Express* **2005**, *13*, 3208.
[18] B. Poumellec, Lancry, A. Chahid-Erraji, P. G. Kazansky, *Opt. Mater. Express* **2011**, *1*, 766.
[19] M. Lancry, B. Poumellec, J. Canning, K. Cook, J.-C. Poulin, F. Brisset, *Laser Photonics Rev.* **2013**, *7*, 953.
[20] C. Hnatovsky, R. S. Taylor, E. Simova, V. R. Bhardwaj, D. M. Rayner, P. B. Corkum, *Opt Lett* **2005**, *230*, 1867.
[21] C. Hnatovsky, R. S. Taylor, P. P. Rajeev, E. Simova, V. R. Bhardwaj, D. M. Rayner, P. B. Corkum, *Appl. Phys. Lett.* **2005**, *87*, 014104.

© 2024 The Authors. Advanced Materials Technologies published by Wiley-VCH GmbH

2365709x, 2024, 18, Downloaded from https://onlinelibrary.wiley.com/doi/10.1002/admt.202400240 by POLITECNICO DI MILANO, Wiley Online Library on [18/09/2024]. See the Terms and Conditions (https://onlinelibrary.wiley.com/terms-and-conditions) on Wiley Online Library for rules of use; OA articles are governed by the applicable Creative Commons License

[22] S. Richter, A. Plech, M. Steinert, M. Heinrich, S. Döring, F. Zimmermann, U. Peschel, E. B. Kley, A. Tünnermann, S. Nolte, *Laser Photonics Rev.* **2012**, *6*, 787.
[23] E. Casamenti, S. Pollonghini, Y. Bellouard, *Opt. Express* **2021**, *29*, 35054.
[24] C. A. Ross, D. G. MacLachlan, D. Choudhury, R. R. Thomson, *Opt. Express* **2018**, *26*, 24343.
[25] M. Ochoa, P. Roldán-Varona, J. F. Algorri, J. M. López-Higuera, L. Rodríguez-Cobo, *Lab Chip* **2023**, *23*, 1752.
[26] L. Bocquet, *Nat. Mater.* **2020**, *19*, 254.
[27] F. Sima, K. Sugioka, *Nanophotonics* **2021**, *10*, 2389.
[28] J. D. Shephard, W. N. MacPherson, R. R. J. Maier, J. D. C. Jones, D. P. Hand, M. Mohebbi, A. K. George, P. J. Roberts, J. C. Knight, *Opt. Express* **2005**, *13*, 7139.
[29] Y. Liao, Y. Cheng, C. Liu, J. Song, F. He, Y. Shen, D. Chen, Z. Xu, Z. Fan, X. Wei, K. Sugioka, K. Midorikawa, *Lab Chip* **2013**, *13*, 1626.
[30] Y. Lu, L. Kai, C. Chen, Q. Yang, Y. Meng, Y. Liu, Y. Cheng, X. Hou, F. Chen, *Adv. Photonics Nexus* **2022**, *1*, 026004.
[31] N. Huot, R. Stoian, A. Mermillod-Blondin, C. Mauclair, E. Audouard, *Opt. Express* **2007**, *15*, 12395.
[32] S. M. Eaton, H. Zhang, P. R. Herman, F. Yoshino, L. Shah, J. Bovatsek, A. Y. Arai, *Opt. Express* **2005**, *13*, 4708.
[33] H. Kogelnik, *BSTJ* **1969**, *48*, 2909.
[34] M. G. Moharam, T. K. Gaylord, *J. Opt Soc. Am.* **1981**, *71*, 811.
[35] J. W. Chan, T. Huser, S. Risbud, D. M. Krol, *Opt. Lett.* **2001**, *26*, 1726.
[36] M. Lancry, B. Poumellec, R. Desmarchelier, B. Bourguignon, *Opt. Mater. Express* **2012**, *2*, 1809.
[37] R. Taylor, C. Hnatovsky, E. Simova, *Laser Photon Rev* **2008**, *2*, 26.
[38] S. Richter, M. Heinrich, S. Döring, A. Tünnermann, S. Nolte, *Appl. Phys. A* **2011**, *104*, 503.
[39] M. Ossiander, M. L. Meretska, H. K. Hampel, S. W. D. Lim, N. Knefz, T. Jauk, F. Capasso, M. Schultze, *Science* **2023**, *380*, 59.
[40] B. Poumellec, L. Sudrie, M. Franco, B. Prade, A. Mysyrowicz, *Opt. Express* **2003**, *11*, 1070.

 © 2024 The Authors. Advanced Materials Technologies published by Wiley-VCH GmbH

2365709x, 2024, 18, Downloaded from https://onlinelibrary.wiley.com/doi/10.1002/admt.202400240 by POLITECNICO DI MILANO, Wiley Online Library on [18/09/2024]. See the Terms and Conditions (https://onlinelibrary.wiley.com/terms-and-conditions) on Wiley Online Library for rules of use; OA articles are governed by the applicable Creative Commons License